Journal of Southeast University (English Edition) Vol. 38, No. 4, pp. 373 – 382 Dec. 2022 ISSN 1003—7985

Impact of a background velocity field on solidification growth of single-crystal nuclei using the PF-LBM

Liang Wenqing [1,2,3] Lei Gang[2] Xun Qining[4] Shu Zhiyong[1,3] Wang Tianxiang[2]
Qian Hua[1] Zhao Dongliang[1] Zheng Xiaohong[1]

([1] School of Energy and Environment, Southeast University, Nanjing 210096, China)
([2] State Key Laboratory of Technologies in Space Cryogenic Propellants, Beijing 100028, China)
([3] State Key Laboratory of Technologies in Space Cryogenic Propellants-SEU Research Center, Nanjing 210096, China)
([4] Shandong Institute of Non-metallic Materials, Jinan 250031, China)

Abstract: To promote/inhibit ice formation in the natural environment and industrial systems, the growth and evolution process of ice single-crystal nuclei were simulated using the phase field-lattice Boltzmann method (PF-LBM), and the influence of a background flow field on the growth of single-crystal nucleus dendrites was also analyzed. The results show that the flow field makes dendrite growth asymmetric. The growth of dendrites is more developed on the upstream side than on the downstream side. The dendrite tip growth rate and tip radius are greater on the upstream side than on the downstream side. The solid phase ratio is greater with a background flow field than without one. The higher the flow velocity is, the more developed the dendrites on the upstream side, the faster the dendrites grow, and the higher the dendrite tip growth rate. The dendrites on the backflow side have a lower flow rate and a lower degree of supercooling than those on the upstream side, which inhibits the solidification process, the growth rate is slow, and the dendrites are underdeveloped.

Key words: single-crystal nucleus; coupled velocity field; simulation; lattice Boltzmann method
DOI: 10.3969/j.issn.1003 – 7985.2022.04.006

Solidification and phase change are well-known processes in industrial production and scientific research. In the process of frost suppression[1], cryogenic food preservation, and other icing processes, and in rocket cryogenic propellant storage, aircraft energy and safety[2], and the energy industry[3], icing is ubiquitous. To reduce potential industrial deterioration and natural disasters, the promotion/inhibition of ice requires an in-depth understanding of the evolution process of water-ice condensation. Studies on the solidification process at room temperature or higher are numerous. However, only a few studies investigate the occurrence of cryogenic crystal condensation, particularly under a flow field. Solidification begins with crystal nuclei formation and then proceeds continuously to form solidified crystals when a background flow field exists.

Many experiments on solidification have been performed to explore dendrites' growth process[4–7]. Huige[4] studied the nucleation and growth of ice crystals in water. Yokoyama et al.[5] investigated the effect of gravity on the tip velocity and radius of ice crystals. Ninagawa et al.[6–7] used high-speed cameras to capture the growth process of ice crystals. Yasuda et al.[8] proposed an improved X-ray electron microscopy technique. However, theoretical and numerical models for directly investigating cryogenic liquids' solidification process remain lacking. Extending the experimental results to cryogenic liquids is expensive and challenging.

With the development of computer technology, numerical simulation has become an efficient alternative method for solving the solidification problem. The commonly used methods to study the solidification process through simulation include Monte Carlo, cellular automata (CA), and phase field (PF) methods. Guo et al.[9] proposed an improved CA-LBM (CA-lattice Boltzmann method), overcoming the grid anisotropy and discrete anisotropy existing in the CA-LBM by improving the differential method. However, the growth of secondary dendrites in the simulation is not apparent, and the simulation is more based on mathematical algorithms, ignoring the actual physical process. With the development of modeling tools, the PF method has a clear physical meaning and high calculation precision and can accurately track the solid-liquid interface used in many metal condensation processes. In addition, better secondary crystal branches are difficult to simulate in the current CA-LBM for the numerical simulation of water crystallization. Although CA has a higher calculation efficiency than the PF method, the simulation of dendrite details by a PF is more ac-

Received 2022-05-06, **Revised** 2022-09-25.
Biographies: Liang Wenqing (1977—), male, doctor, lecturer; Zheng Xiaohong (corresponding author), female, doctor, associate professor, xhzheng@seu.edu.cn.
Foundation item: The National Key Research and Development Program of China (No. 2020YFB1506203).
Citation: Liang Wenqing, Lei Gang, Xun Qining, et al. Impact of a background velocity field on solidification growth of single-crystal nuclei using the PF-LBM[J]. Journal of Southeast University (English Edition), 2022, 38(4): 373 – 382. DOI: 10.3969/j.issn.1003 – 7985.2022.04.006.

curate and closer to the Lipton-Glicksman-Kurz (LGK) theoretical solution. The PF-LBM calculates the solid-liquid interface more accurately than other models. Kobayashi[10] uses a PF model to simulate the dendritic growth of pure metals in undercooled melts under two-dimensional conditions. Wheeler et al.[11] use a model proposed by Penrose et al.[12] to calculate the solidification process of Ni. The calculated results agree well with Ivanovo's theory. Wheeler et al.[13] further developed the binary alloy PF model. Kim et al.[14] proposed a PF model suitable for dilute solution. Qin et al.[15] developed a multi-element alloy solidification model to predict the solidification process of a four-element alloy, which agrees well with the experimental results. Luo et al.[16] used the PF-LBM to predict the growth and movement of dendrites in a Fe-C alloy solution. Some studies investigate dendrites' growth with a background flow field by fixing the positions of dendrites in the computational domain and ignoring the movement of dendrites in the flow field. Previous literature shows that the supercooling and velocity of the background flow field can have important effects on solidification. Therefore, the PF-LBM proposed in the study simulates the ice crystal solidification by the PF model, and the LBM simulates the flow field motion, thus realizing a coupled simulation. The LBM is widely used to simulate mesoscale thermal fluid or chemical reactions[17-20]. However, the theoretical study of ice dendrite based on ice dendrite growth analysis fails to capture the growth interaction between the dendrite arms, which cannot be ignored in the process of dendrite icing. In addition, studies are lacking on dendrite growth and the movement of water in cryogenic environments. The study of ice condensation processes and the shape of ice in cryogenic environments can be a great guide for industries to inhibit or promote ice production.

The goal of this paper is to predict the dendrite growth and condensation process of water and water vapor in a cryogenic environment. The CA-LBM is used to overcome the grid anisotropy in cartesian coordinates to simulate the microscopic dendritic growth process of water under a certain degree of supercooling. However, the sixfold dendrite structure is too imprecise, and the secondary dendrite is too subtle. The PF-LBM can accurately track the solid-liquid interface, enabling more accurate secondary graft shapes and growth rates to be obtained. The coupling of the PF-LBM was developed and used in this paper to predict the process. In this paper, not only the dendrite structure and tip velocity of ice crystals under the flow field are simulated, but also the secondary dendrite morphology is more obvious.

1 Method

1.1 PF

According to the Ginzburg-Landau free energy theory, the expression for the free energy F of a closed system is

$$F = \int_{\Omega} \left[f(\varphi, T) + \frac{1}{2} \varepsilon^2 | \nabla \varphi |^2 \right] \mathrm{d}\Omega \tag{1}$$

where $f(\varphi, T)$ is the free energy density function; φ is the PF parameter; T is the temperature; and ε is the anisotropic kinetic coefficient.

According to the second law of thermodynamics, the free energy of an isolated system continuously decreases to the equilibrium state, that is, $\mathrm{d}F \leqslant 0$. From the Ginzburg-Landau equation, the time evolution equation satisfying the condition of $\mathrm{d}F \leqslant 0$ is

$$\xi \frac{\partial \varphi}{\partial t} = -\frac{\delta F}{\delta \varphi} \tag{2}$$

where ξ is a parameter related to interface dynamics. The PF control equation based on the free energy density function model is

$$\xi \frac{\partial \varphi}{\partial t} = \varepsilon^2 \nabla^2 \varphi + 2\varphi(1-\varphi)\left(2\varphi - 1 - 4\lambda(1-\varphi)(T - T_{\mathrm{M}})\right) \tag{3}$$

The temperature field control equation is

$$\frac{\partial T}{\partial t} = D_T \nabla^2 T + \frac{L \partial h(\varphi)}{C_p \partial t} \tag{4}$$

The anisotropic kinetic coefficient ε can be expressed as a function of the angle θ between the preferred growth angle and the interface normal direction:

$$\left.\begin{aligned} \varepsilon(\theta) &= \varepsilon_0 \alpha_s(\theta) = \varepsilon_0 (1 + \gamma \cos\lambda\theta) \\ \tau(\theta) &= \tau_0 \alpha_s^2(\theta) = \tau_0 (1 + \gamma \cos\lambda\theta)^2 \end{aligned}\right\} \tag{5}$$

where ε_0 is the constant interface thickness; $\alpha_s(\theta)$ is the anisotropy factor; γ is the anisotropy index, which is 0.02; λ is the anisotropy modulus, which is 6 in this article[21];

$$\tan\theta = \frac{\partial \varphi / \partial y}{\partial \varphi / \partial x} \tag{6}$$

1.2 LBM

The shape of the solid-liquid interface is complex and difficult to track. The lattice Boltzmann equation is a special discretization format. The discretization includes velocity discretization, time discretization, and space discretization obtained from

$$f_\alpha(\boldsymbol{r} + \boldsymbol{e}_\alpha \delta t, t + \delta t) - f_\alpha(\boldsymbol{r}, t) = \frac{1}{\tau}\left[f_\alpha^{\mathrm{eq}}(\boldsymbol{r}, t) - f_\alpha(\boldsymbol{r}, t)\right] \tag{7}$$

where $\boldsymbol{e}_\alpha$ is the dispersion of velocity; δt is the time step; t is the dimensionless relaxation time; τ is the relaxation factor, $\tau = \frac{3\nu}{\delta t} + 0.5$, and ν is the kinematic viscosity.

The lattice Boltzmann model comprises three parts: the discrete velocity model of the lattice, the distribution function of equilibrium, and the evolution equation of the dis-

tribution function. These three parts will be introduced separately below. For the discrete velocity model, the discrete velocity configuration of the D2Q9 model is as follows:

$$\boldsymbol{e}_\alpha = \begin{cases} (0,0) & \alpha = 0 \\ c(\cos[(\alpha-1)\pi/2], \sin[(\alpha-1)\pi/2]) & \alpha = 1,2,3,4 \\ \sqrt{2}c(\cos[(2\alpha-1)\pi/4], \sin[(2\alpha-1)\pi/4]) & \alpha = 5,6,7,8 \end{cases} \tag{8}$$

where c represents the grid speed, that is, the ratio of the grid step to the time step. In general, $c = 1$. The velocity model indicates that the particles in the nine grids can move in different directions to the neighboring grid points according to the speed c, except for staying at the original grid point.

In the D2Q9 model proposed by McNamara et al.[22], the equilibrium distribution function expression is as follows:

$$f^{\mathrm{eq}} = \rho\omega_\alpha\left[1 + \frac{\boldsymbol{e}_\alpha \cdot \boldsymbol{u}}{c_s^2} + \frac{(\boldsymbol{e}_\alpha \cdot \boldsymbol{u})^2}{2c_s^4} - \frac{\boldsymbol{u}^2}{2c_s^2}\right] \tag{9}$$

where ρ is macroscopic fluid density; $\boldsymbol{u}$ is the macroscopic fluid velocity; c_s is the lattice sound velocity; and w_α is the weight coefficient.

The macroscopic fluid density and macroscopic fluid velocity of the model are defined as follows:

$$\rho = \sum_\alpha f_\alpha \tag{10}$$

$$\boldsymbol{u} = \frac{1}{\rho}\sum_\alpha f_\alpha \boldsymbol{e}_\alpha \tag{11}$$

The weight coefficients of the D2Q9 model used in this article are

$$\omega_\alpha = \begin{cases} 4/9 & \alpha = 0 \\ 1/9 & \alpha = 1,2,3,4 \\ 1/36 & \alpha = 5,6,7,8 \end{cases} \tag{12}$$

In this paper, the temperature boundary of the calculation domain is an adiabatic boundary condition (zero Neumann boundary condition); that is, the heat flux density on the boundary is zero, $\partial u/\partial t = 0$. The velocity entrance and exit adopt the nonequilibrium rebound format of the dynamic format[23]. The solid-liquid interface is assumed as a non-slip fluid boundary, and fluid particles cannot penetrate the solid-liquid interface via diffusion. Thus, the boundary conditions of the bounce-back format are adopted for the wall surface (including the solid-liquid interface). The core idea of the bounce-back format is to rebound the particles on the boundary. When the particles on the fluid node reach the boundary, they return along the original path.

The temperature field is given as follows:

$$g_\alpha(x + \boldsymbol{e}_\alpha\delta t, t + \delta t) - g_\alpha(\boldsymbol{x}, t) = \frac{1}{\tau_{\mathrm{T}}}\left(g^{\mathrm{eq}}(x,t) - g_\alpha(\boldsymbol{x},t)\right) + \delta t\omega_\alpha\Phi_x \tag{13}$$

where τ_{T} is the relaxation time calculated by

$$\tau_{\mathrm{T}} = 3\alpha + 0.5 \tag{14}$$

where α is the thermal diffusivity. *Φ_x is the source term. Thus*,

$$\Phi_x = f_s\boldsymbol{x} - f_s^0\boldsymbol{x}\frac{L}{c_p} \tag{15}$$

where L is the latent heat of solidification; and $f_s^0(\boldsymbol{x})$ is the solid fraction at node $\boldsymbol{x}$ from the previous time step.

The equilibrium temperature distribution function is obtained by

$$g_\alpha^{\mathrm{eq}}(\boldsymbol{x}, t) = \omega_\alpha T + \frac{\boldsymbol{e}_\alpha \cdot \boldsymbol{u}}{c_s^2} + \frac{(\boldsymbol{e}_\alpha \cdot \boldsymbol{u})^2}{2c_s^4} - \frac{\boldsymbol{u}^2}{2c_s^2} \tag{16}$$

The temperature of a certain component is calculated by

$$T = \sum_i g_i \tag{17}$$

1.3 Coupling of PF and LBM

The temperature and velocity distribution of the solidification field are obtained through an LBM calculation, and then the PF method is used to calculate the dendrite growth velocity according to the temperature distribution of the solid-liquid interface. As the solidification progresses, the latent heat released at the front of the dendrite will be added as a source term to the evolution equation of the LBM. In this manner, PF-LBM achieves mutual coupling and realizes dendrite growth under the action of a simulated flow field. The specific calculation process is shown in Fig. 1.

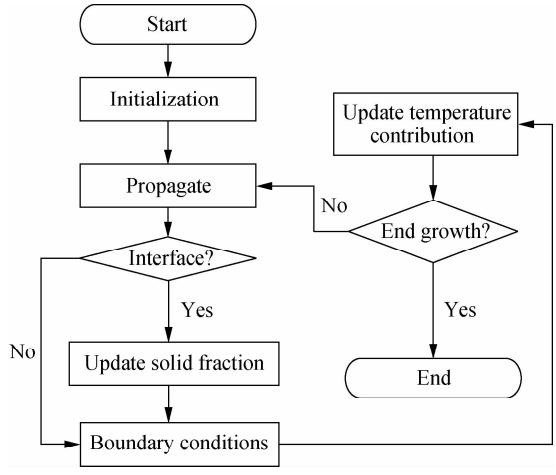

Fig. 1 Overall flowchart for PF-LBM analysis

This study simulated the solidification process of water in refrigerant R410a. The physical parameters of ice are shown in Tab. 1. The simulation area is divided into 300 × 300 uniform grids with a grid size of $\Delta x = 0.1$ mm, a time step of $\Delta t = 20$ μs, a crystal nucleus is set at the center of the grid at the initial time, and the radius of the crystal nucleus is four grids. The supercooled fluid in the

calculation area enters from the left boundary and flows out from the right boundary at a speed of u. The crystal nucleus is located at the center of the simulation area, as shown in Fig. 2.

Tab. 1 Properties of the numerical model

Property	Value
Density ρ/(kg ·m^{-3})	1 000
Thermal diffusivity α/(mm^2 ·s^{-1})	0.222
Latent heat of solidification L/(kJ ·kg^{-1})	335
Specific heat capacity at constant pressure c_p/(kJ ·kg^{-1} ·K^{-1})	2.1
Prandtl number Pr	13.474
Average kinetic coefficient $\mu_{k0}/10^{-3}$	8
Anisotropic kinetic coefficient ε_μ	0.35

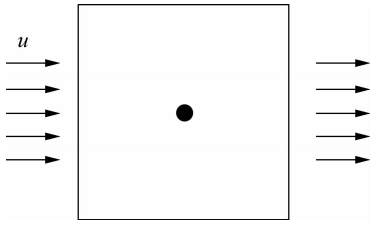

Fig. 2 Flow diagram of a single grid with a crystal nucleus set at the center

2 Results

2.1 Validation of the proposed model

To explore the reliability of dendrite growth under a flow field, the simulation results were compared with the experimental results. Bouissou et al.[24] studied the effect of the flow field on the solidification process of trimethylacetic acid using experimental methods. Because of the high freezing point of trimethylacetic acid, this experiment can be performed at room temperature. As shown in Fig. 3(a), the flow rate affects the shape of the solidification. In this case, the external hydrodynamic velocity is 19 times the crystal growth velocity. One observes that side branching develops asymmetrically along the sides: it is enhanced on the side more directly subjected to the influence of the external flow and inhibited on the other side. The external flows tend to favor side branching development. In the case of no flow, the steady rate of growth of crystal branches is 35 μm^3/s. Notably, for an external flow field U = 15 μm/s, the crystal branches grow at a steady rate of 55 μm^3/s[24]. Dendrites grow on the flow surface as a result of the incoming flow and outgoing flow. The secondary dendrite growth is more developed on the front flow surface and small on the backflow surface. Fig. 3(b) shows the dendrite growth calculated by the PF-LBM described in this article, and the direction of the incoming flow velocity is consistent with Bouissou's experiment. The results of simulation calculations in Fig. 3(b) show that the growth of dendrites in the upstream direction is developed, the secondary dendrites are large, and the secondary dendrites grow slowly and not very clearly on the backflow surface. Comparing Fig. 3(a) and Fig. 3(b) indicates that the simulation results in this paper are approximately the same as the experimental results, verifying the coupled PF and flow field models.

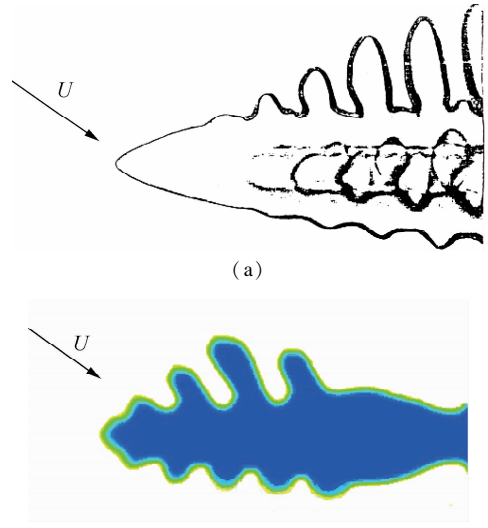

Fig. 3 Growth shape of dendrites. (a) Experiment; (b) Simulation

LGK theory assumes that the dendrite tip is an ideal smooth parabola. The total subcooling during crystallization is expressed as a function of the dendrite growth rate and tip radius combined with the Ivantsov function[25]:

$$\Delta T = \mathrm{Iv}(P_t)\frac{\Delta H}{c_p} + m_1 c_0\left(1 - \frac{1}{1-(1-k_0)\mathrm{Iv}(P_c)}\right) + \frac{2\Gamma}{R} \tag{18}$$

where k_0 is the solute distribution coefficient; Γ is the Thomson-Gibbs coefficient; P_t and P_c are the temperature Peclet number $P_t = vR/(2a)$ and the concentration Peclet number $P_c = vR/(2D)$, respectively. The Ivantsov function combined with the Peclet number can accurately represent the temperature and concentration transfer process:

$$\mathrm{Iv}(P) = P\exp(P)E(P) \tag{19}$$

$$E_1(P) = \int_P^\infty \frac{\mathrm{e}^{-x}}{x}\mathrm{d}x \tag{20}$$

The values of v and R determined only with Eq. (20) are insufficient; therefore, the stability criterion factor σ^* is introduced into the theory:

$$R = \left[\frac{\Gamma}{\sigma^*(m\overline{G}_c - \overline{G})}\right]^{1/2} \tag{21}$$

where $\overline{G_c}$ and $\overline{G}$ represent the average concentration gradient and average temperature gradient of the interface, respectively.

To verify the accuracy of the PF-LBM, the steady

growth of dendrite is compared with the theoretical result of the LGK method[25], as shown in Fig. 4. Initially, because of the lower interface concentration, the dendrite growth rate is faster. In addition to inhibiting dendrite growth, the rejected solute and the latent heat tend to stabilize the growth as the solidification progresses. Fig. 4 shows that the equilibrium dendrite growth is near the theoretical value obtained from the LGK method.

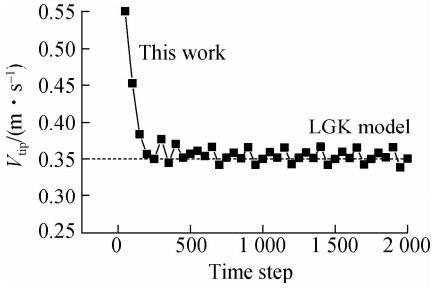

Fig. 4 Comparison and verification of simulation results and the LGK model

2.2 Morphology evolution of the solidification process in the presence and absence of a flow field

The growth morphologies of dendrites were compared with and without a flow field. Fig. 5 compares dendritic growth at 10 ms with and without the flow field. Figs. 5 (a) and (b) show the morphology of dendritic growth in the absence of the flow field and when the flow velocity is 0.2 m/s, respectively. According to Fig. 5, the presence of the flow field changes the original growth morphology of dendrites, and the dendrites are more developed on the inflow side than on the outflow side. The simulation results of this study are approximately consistent with the experimental results, and the model of the coupled PF and flow field has been verified[24]. Because the subcooled fluid scours the dendrites on the upstream side, a large amount of heat is transferred to the downstream side, reducing the thickness of the interfacial layer on the upstream side, thus causing the actual subcooling on the upstream side to increase and the dendrites to grow rapidly. However, a large amount of heat accumulates on the backflow side, and the low flow rate on the backflow side prevents heat from being discharged in time, resulting in an undersized temperature gradient, thus inhibiting dendritic growth. Fig. 6(a) shows the cloud chart of the velocity field distribution under the condition of Fig. 5 (b). Fig. 6(a) shows that the velocity on the backflow side is approximately 0.06 to 0.1 m/s, which is lower than the inlet velocity. Fig. 6 (b) is the temperature field distribution diagram under the condition of Fig. 5 (b). It can be seen that the temperature gradient is larger on the upstream side and smaller on the downstream side, thus promoting the solidification process growth on the upstream side and inhibiting it on the downstream side.

Fig. 5(c) shows the main characteristics of the nucleation and growth process of ice crystals in the cryoprotectant observed by Tao et al.[26] under a cryomicroscope. The experimental results show that with the continuous growth of ice crystals, the crystal nucleus gradually becomes larger and presents a hexagon. At each tip of the hexagon, a crystal axis grows out, forming a backbone of the crystal axis, which is on the crystal axis. A secondary dendrite crystal axis grows out. The final shape and structure of the ice crystals evolved into snowflake-shaped equiaxed dendrites. The experimental results agree well with the morphological evolution characteristics of the ice crystals simulated in Figs. 5 (a) and (b).

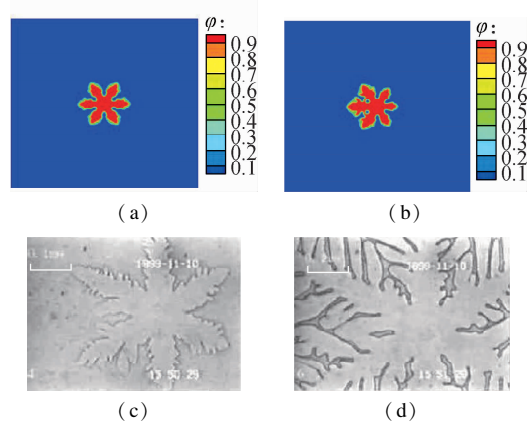

Fig. 5 Comparison of dendrite growth morphology at the same solidification time t = 15 ms. (a) Static flow field; (b) Dynamic flow field; (c) Ice crystal growth under a cryomicroscope; (d) Dendritic ice crystal under a cryomicroscope[26]

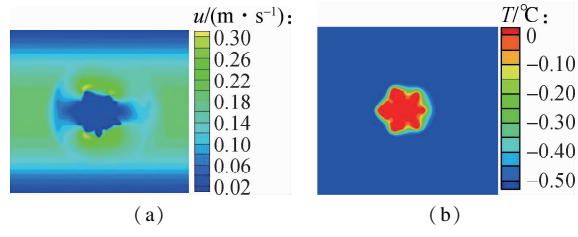

Fig. 6 Cloud chart. (a) Velocity; (b) Temperature field distribution chart

Fig. 7 is the shape change diagram of the dendrite growth process. At the beginning of dendrite growth, the upstream side is more developed than the downstream side. Secondary dendrites begin to appear on the main crystal axis with time elapsing. Figs. 7 (c) and (d) reveal that the secondary dendrites are much more developed on the upstream side than on the downstream side, and almost no secondary dendrites are present on the main crystal axis on the downstream side. This result is due to the low flow velocity on the backflow side, which prevents the heat from being discharged in time, resulting in an undersized temperature gradient, thus inhibiting dendritic growth. The results show that the secondary dendrites will be finer and denser with increasing supercoo-

ling degrees. As a result of the continuous impact of cold fluid on the upstream side, the supercooling degree is higher on the downstream side, so the growth shapes of secondary dendrites on both sides show obvious differences, which are caused by different supercooling degrees.

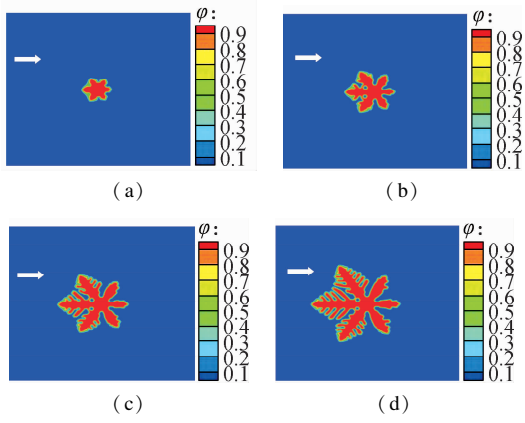

Fig. 7 Dendritic crystal changes with time under dynamic flow field conditions. (a) t = 5 ms; (b) t = 10 ms; (c) t = 15 ms; (d) t = 20 ms

Fig. 8 is a graph of the dendritic tip growth rate V_{tip} and the tip radius of curvature R_{tip} versus time on the upstream and downstream sides during dendritic growth. As shown, the dendrite tip growth rate is greater on the upstream side than on the downstream side, the average growth rate is 0.45 and 0.23 m/s on the upstream and downstream sides, respectively, and the growth rate on the upstream side is about twice that on the downstream side. As also shown, the tip radius is larger on the upstream side than on the downstream side, and the average tip radius is 6.5 mm on the upstream side and 5.5 mm on the downstream side. According to the research of Guo et al. [9], a larger tip velocity was found in the first few time steps of the initial stage (t < 0.3 s). Because of the balance between the heat generated by the phase change and the heat diffused in the ice and water, the tip velocity is almost constant, with very small fluctuations (0.3 s < t < 1.0 s). In the initial stage, the growth rate of the tip of the crystal branch is high, and the decay rate is high. Since the temperature difference at this time is large, and the surrounding temperature field changes as the crystal branches grow, the growth rate of the tips of the crystal branches becomes stable.

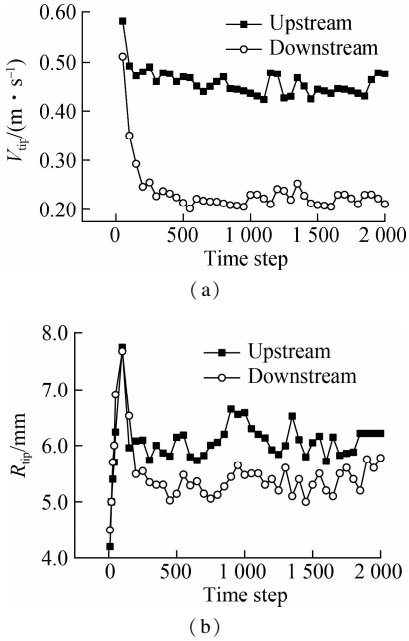

Fig. 8 Growth rate V_{tip} and radius of curvature R_{tip} of dendrite tips on the upstream and downstream sides versus time during dendrite growth. (a) Velocity of dendritic tip growth; (b) Tip curvature radius

The solid phase ratio ϕ is defined as the solidified calculation area compared to the total calculation area. Fig. 9 is a graph showing the change in the solid phase ratio with time during dendritic growth in the presence of a flow field. As seen from Fig. 9, consistent with the calculation results in the previous paragraphs, the solid phase ratio also increases with the calculation time step. At the same time, the change curves of the solid phase ratio under the same conditions without the flow field are compared. The results show a larger solid phase ratio under the flow field than under the no flow field. Greater changes in dendrite morphology occur under the flow field. On the inflow side, the dendrite becomes larger, and on the backflow side, because of the presence of an eddy current, dendrite growth is also promoted.

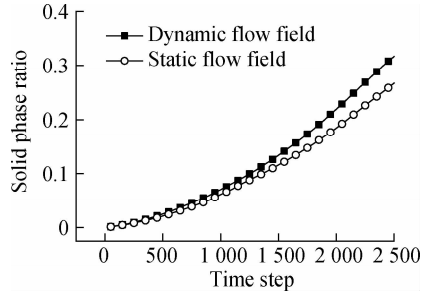

Fig. 9 Changes in the solid phase ratio with time under static and dynamic flow fields

2.3 Effect of solidification growth morphology and solid phase ratio at different flow rates

Under the same conditions, different velocities have different effects on the appearance of dendrites. Figs. 10 (a), (b), (c), and (d) are PF distribution diagrams when the flow velocities are u = 0.10, 0.15, 0.20, and 0.25 m/s, respectively, and t = 1 000 or 20 ms. As shown in Fig. 10, the greater the inflow speed is, the more obvious the asymmetry of dendrite morphology, which changes the original symmetrical growth morphology. The higher the velocity, the faster the dendrite

growth on the upstream side, and the more developed the secondary dendrite. However, the growth rate of the main crystal axis on the backflow side decreases with increasing flow rate, and the secondary dendrites are also less developed. When the flow velocity is $u = 0.25$ m/s, the growth of the main crystal axis on the upstream side is the most developed, and the secondary dendrites are also the most developed. The difference between the upstream and back sides is the largest, and the growing inclination is the most obvious. When $u = 0.10$ m/s, the dendritic growth on the upstream side is slower than that on the downstream side at other flow rates, and the dendritic growth on the downstream side is more developed than that at other flow rates. Therefore, under the same solidification time and within a certain flow rate range, the higher the flow rate is, the more developed the dendritic growth on the upstream side, while the dendritic growth on the downstream side is weakened with increasing flow rate. The ice crystal tip velocity is promoted by the natural convection of the dendrite arms opposite to the direction of gravity, while the dendrite arms in the direction of gravity are suppressed[9], which is consistent with the experimental results of Koo et al[27]. The greater the velocity of the external flow field is, the more obvious the enhancement effect on the front flow and the suppression effect on the backflow. This simulation uses the PF-LBM to simulate the secondary crystal dendrite result of ice crystal condensation, which is better than the CA-LBM of Guo et al[9], and from the results of forced convection conditions, it also meets the experimental results of Koo et al[27]. Additionally, Fig. 10 shows that the weakening of the tip growth on the dorsal side is greater than the enhancement on the forward side, which is consistent with the findings of Sakane et al[28]. Moreover, the simulation found that the secondary crystal branches on the backflow side virtually disappeared.

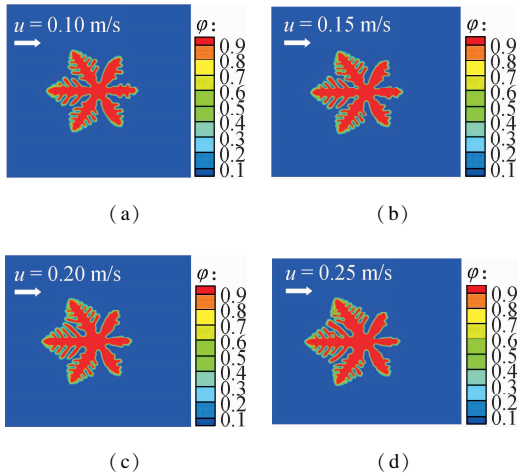

Fig. 10 Dendrite appearance at different flow rates when t = 1 000 ms. (a) $u = 0.10$ m/s; (b) $u = 0.15$ m/s; (c) $u = 0.20$ m/s; (d) $u = 0.25$ m/s

Fig. 11 shows a graph of dendritic tip growth rate V_{tip} and tip radius of curvature R_{tip} versus time at different flow rates on the upstream and downstream sides. At the same flow rate, the dendrite tip growth rate and tip radius are greater on the upstream side than on the downstream side. For different flow rates, with increasing flow rates, the dendritic tip growth rate increases on the upstream side and decreases on the downstream side. Fig. 11(a) reveals that when $u = 0.25$ m/s, the growth rate of the dendrite tip is the largest on the upstream side and the smallest on the downstream side, and the difference between the two rates is the largest. At $u = 0.10$ m/s, the dendrite tip growth rate is the smallest on the upstream side and the largest on the downstream side, and the difference between the two sides is the smallest. According to the results, the higher the flow rate is, the higher the dendritic tip growth rate on the upstream side and the lower the dendritic tip growth rate on the downstream side. The higher the flow rate is, the greater the temperature gradient on the upstream side, and the heat on the upstream side can be quickly released so that the thermal energy is more concentrated on the downstream side and dendritic growth on the downstream side is inhibited. Additionally, regarding the tip radius of curvature, Fig. 11(b) shows that the greater the flow rate is, the larger and smaller the tip radius of curvature on the upstream and downstream sides, respectively. The higher the flow rate is, the higher and lower the growth rate of the dendrite tip on

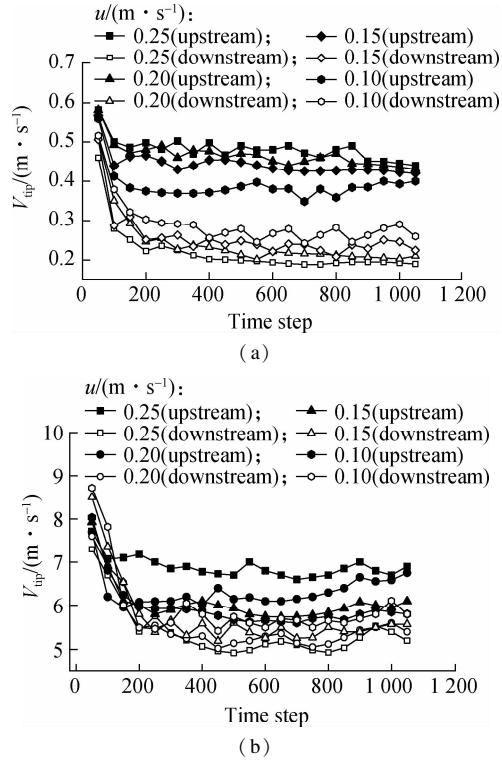

Fig. 11 Comparison of dendritic tip growth rate V_{tip} and tip radius R_{tip} on the upstream side and the downstream side at different speeds. (a) Velocity of dendritic tip growth; (b) Tip curvature radius

the upstream and downstream sides, respectively, thus causing a larger tip radius of curvature on the upstream side and a smaller tip radius on the downstream side. The higher the flow rate is, the greater the temperature gradient on the upstream side, which can quickly remove the heat on the upstream side, promote the growth of the tip, and increase the radius of curvature. At the same time, the thermal energy is more concentrated on the backflow side, the dendritic growth on the backflow side is inhibited, and the curvature radius of the tip on the backflow side is reduced.

Under a flow field within a certain range, the larger the flow rate is, the larger the solid phase ratio. Fig. 12 is a graph showing the change in solid phase ratio with time at different flow rates. It shows that dendritic growth is promoted by the flow on the upstream side and inhibited on the downstream side. Generally speaking, the higher the flow rate is, the higher the solid phase ratio at the same time. As shown, the presence of a flow field promotes solidification. Although the flow field inhibits the downstream dendrite growth, the promotion effect on the upstream dendrite is stronger. At the early stage of solidification, the flow velocity has a limited effect on the solid phase fraction because the promotion and inhibition effects of the flow field on the upstream and downstream dendrite, respectively, have not yet appeared; thus, the asymmetry of dendrite growth is not large. However, the asymmetry of dendritic growth becomes prominent, and the effect of flow velocity becomes increasingly more obvious as the solidification progresses.

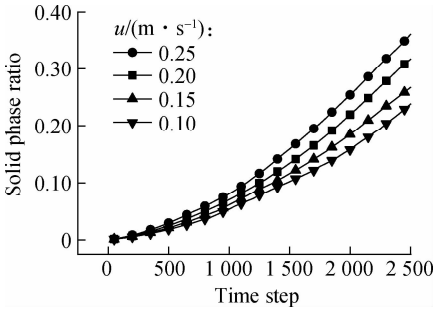

Fig. 12 Relationship between the solid phase ratio and time under different flow rates

2.4 Effect of undercooling on the solidification process of crystal nuclei

The degree of undercooling has an important influence on the solidification growth process. To study the influence of the degree of subcooling on the crystal growth process, different degrees of subcooling were selected for simulation calculations in this section, and the degrees of subcooling were 0.40, 0.45, 0.50, and 0.55, respectively. The simulation results are shown in Fig. 13. In the same simulation time, when the degree of subcooling is small, the resulting crystal morphology is small, the crystal backbone is thicker, and secondary dendrites are inconspicuous on the main branches. With increasing undercooling, the crystal morphology becomes larger, and the crystal backbone becomes thinner and longer with obvious secondary branches. As the degree of supercooling continues to increase, the crystal morphology becomes larger, the main stem is slenderer, and the secondary branches are developed. This result shows that the degree of undercooling obviously affects the growth rate and final morphology of the solidification process. A large degree of undercooling can promote the solidification process and the growth of secondary branches, and the growth of secondary dendrite arms makes the dendrite trunk thinner, which is consistent with the continuous growth mechanism of crystals in solidification theory. Figs. 13(e) and (f) show the experimentally observed ice crystal shapes under different subcooling conditions[26]. Under large undercooling, the six main crystal axes are thinner, and the secondary dendrite arms on the main crystal axis are thinner. In addition, under large undercooling, the secondary dendrite arms are finer and more numerous, which is consistent with the calculated results of the theoretical model.

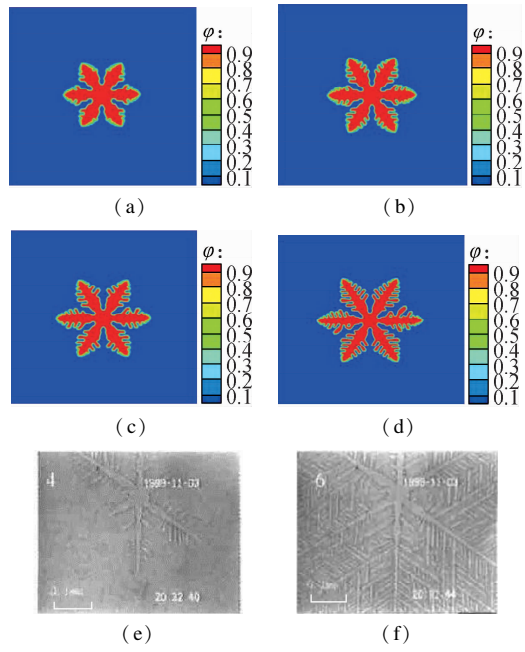

Fig. 13 Dendrite appearance under different undercoolings when $t = 1\,000$ ms. (a) Degree of subcooling 0.40; (b) Degree of subcooling 0.45; (c) Degree of subcooling 0.50; (d) Degree of subcooling 0.55; (e) Small undercooling; (f) Large overcooling

3 Conclusions

1) The solidification growth process in the presence of a flow field is simulated. The results show that the existence of a flow field makes dendrites grow asymmetrically. The dendrite growth is more developed on the upstream side than on the downstream side. There are obvious secondary dendrites on the upstream side. The dendrite tip growth rate is greater on the upstream side than

on the downstream side, and the tip radius is greater on the upstream side than on the downstream side.

2) Because of the flow field's presence, dendritic growth is promoted on the upstream side and inhibited on the downstream side. The presence of the flow field increases the solid phase ratio. The solid phase ratio increases because the supercooled fluid continuously removes heat.

3) The effects of different flow rates on dendrite growth during solidification are compared. The simulation results show that the higher the flow rate is, the more developed the dendrite on the upstream side, the faster the dendrite growth, and the higher the dendrite tip growth rate; thus, the higher the solid phase ratio at the same time. However, on the backflow side, the solidification process of dendrites is inhibited, the growth rate is low, and the dendrites are less developed than those on the front flow side because of the small flow velocity and the lower supercooling degree.

References

[1] Qian J F, Zhang J L. Feasibility analysis of urban sewage source heat pump system with freezing latent heat collection[J]. *Journal of Southeast University (English Edition)*, 2010(2): 324-326. DOI: 10.3969/j.issn.1003-7985.2010.02.040.

[2] Cao Y H, Tan W Y, Wu Z L. Aircraft icing: An ongoing threat to aviation safety[J]. *Aerospace Science and Technology*, 2018, **75**: 353-385. DOI: 10.1016/j.ast.2017.12.028.

[3] Li Q, Sun G X, Luo S, et al. Evaluation of rutting and low-temperature cracking resistances of warm-mix recycled asphalt binders under the secondary aging condition [J]. *Journal of Southeast University (English Edition)*, 2020, **36**(1): 81-87. DOI: 10.3969/j.issn.1003-7985.2020.01.011.

[4] Huige N. *Nucleation and growth of ice crystals from water and sugar solutions in continuous sturred tank crystallizers*[D]. Eindhoven, The Kingdom of the Netherlands: Eindhoven University of Technology, 1972.

[5] Yokoyama E, Yoshizaki I, Shimaoka T, et al. Measurements of growth rates of an ice crystal from supercooled heavy water under microgravity conditions: Basal face growth rate and tip velocity of a dendrite[J]. *The Journal of Physical Chemistry B*, 2011, **115**(27): 8739-8745. DOI: 10.1021/jp110634t.

[6] Ninagawa T, Eguchi A, Kawamura Y, et al. A study on ice crystal formation behavior at intracellular freezing of plant cells using a high-speed camera[J]. *Cryobiology*, 2016, **73**(1): 20-29. DOI: 10.1016/j.cryobiol.2016.06.003.

[7] Kielar J J, Lemaitre P, Gobin C, et al. Simultaneous interferometric in-focus and out-of-focus imaging of ice crystals[J]. *Optics Communications*, 2016, **372**: 185-195. DOI: 10.1016/j.optcom.2016.04.004.

[8] Yasuda H, Yamamoto Y, Nakatsuka N, et al. In situ observation of solidification phenomena in Al-Cu and Fe-Si-Al alloys[J]. *International Journal of Cast Metals Research*, 2009, **22**(1/2/3/4): 15-21. DOI: 10.1179/136404609X368118.

[9] Guo Q, Cheng P. Numerical investigations of six-fold dendritic icing process in subcooled water subject to natural and forced convective environments[J]. *International Journal of Heat and Mass Transfer*, 2019, **145**: 118658. DOI: 10.1016/j.ijheatmasstransfer.2019.118658.

[10] Kobayashi R. Modeling and numerical simulations of dendritic crystal growth[J]. *Physica D: Nonlinear Phenomena*, 1993, **63**(3/4): 410-423. DOI: 10.1016/0167-2789(93)90120-P.

[11] Wheeler A A, Murray B T, Schaefer R J. Computation of dendrites using a phase field model[J]. *Physica D: Nonlinear Phenomena*, 1993, **66**(1/2): 243-262. DOI: 10.1016/0167-2789(93)90242-S.

[12] Penrose O, Fife P C. Thermodynamically consistent models of phase-field type for the kinetic of phase transitions[J]. *Physica D: Nonlinear Phenomena*, 1990, **43**(1): 44-62. DOI: 10.1016/0167-2789(90)90015-H.

[13] Wheeler A A, Boettinger W J, McFadden G B. Phase-field model for isothermal phase transitions in binary alloys[J]. *Physical Review A, Atomic, Molecular, and Optical Physics*, 1992, **45**(10): 7424-7439. DOI: 10.1103/physreva.45.7424.

[14] Kim S G, Kim W T, Suzuki T. Phase-field model for binary alloys[J]. *Physical Review E*, 1999, **60**(6): 7186-7197. DOI: 10.1103/physreve.60.7186.

[15] Qin R S, Wallach E R, Thomson R C. A phase-field model for the solidification of multicomponent and multiphase alloys[J]. *Journal of Crystal Growth*, 2005, **279**(1/2): 163-169. DOI: 10.1016/j.jcrysgro.2005.02.005.

[16] Luo S, Wang P, Wang W L, et al. PF-LBM modelling of dendritic growth and motion in an undercooled melt of Fe-C binary alloy[J]. *Metallurgical and Materials Transactions B*, 2020, **51**(5): 2268-2284. DOI: 10.1007/s11663-020-01925-6.

[17] Kan A K, Mao S, Wang N, et al. Simulation and experimental study on thermal conductivity ofnano-granule porous material based on lattice-boltzmann method [J]. *Journal of Thermal Science*, 2021, **30**(1): 248-256. DOI: 10.1007/s11630-019-1218-1.

[18] Taher M A, Kim H D, Lee Y W. Study of thermal and hydraulic performances of circular and square ribbed rough microchannels using LBM[J]. *Journal of Thermal Science*, 2015, **24**(6): 549-556. DOI: 10.1007/s11630-015-0821-z.

[19] Xin F, Li X F, Xu M, et al. Simulation of gas exothermic chemical reaction in porous media reactor with latticeBoltzmann method[J]. *Journal of Thermal Science*, 2013, **22**(1): 42-47. DOI: 10.1007/s11630-013-0590-5.

[20] Yang B, Wu W, Li M D, et al. A multiple-relaxation-time lattice Boltzmann model for natural convection in a hydrodynamically and thermally anisotropic porous medium under local thermal non-equilibrium conditions[J]. *Journal of Thermal Science*, 2020, **29**(3): 609-622. DOI: 10.1007/s11630-020-1169-6.

[21] Alexandrov D V, Galenko P K. Dendritic growth with

the six-fold symmetry: Theoretical predictions and experimental verification[J]. *Journal of Physics and Chemistry of Solids*, 2017, **108**: 98 - 103. DOI:10.1016/j.jpcs.2017.04.016.

[22] McNamara G R, Zanetti G. Use of the Boltzmann equation to simulate lattice gas automata[J]. *Physical Review Letters*, 1988, **61**(20): 2332 - 2335. DOI:10.1103/PhysRevLett.61.2332.

[23] Zou Q S, He X Y. On pressure and velocity boundary conditions for the lattice Boltzmann BGK model[J]. *Physics of Fluids*, 1997, **9**(6): 1591 - 1598. DOI:10.1063/1.869307.

[24] Bouissou P, Perrin B, Tabeling P. Influence of an external flow on dendritic crystal growth[J]. *Physical Review A*, 1989, **40**(1): 509 - 510. DOI:10.1103/physreva.40.509.

[25] Lipton J, Glicksman M E, Kurz W. Dendritic growth into undercooled alloy metals[J]. *Materials Science and Engineering*, 1984, **65**(1): 57 - 63. DOI:10.1016/0025-5416(84)90199-X.

[26] Tao L R, Hua Z Z. A microscopic study of the crystallization in cryoprotectent agents[J]. *Journal of Engineering Thermophysics*, 2001(4): 481 - 484. DOI: 10.3321/j.issn:0253-231X.2001.04.025. (in Chinese)

[27] Koo K K, Ananth R, Gill W N. Thermal convection, morphological stability and the dendritic growth of crystals[J]. *AIChE Journal*, 1992, **38**(6): 945 - 954. DOI:10.1002/aic.690380615.

[28] Sakane S, Takaki T, Ohno M, et al. Three-dimensional morphologies of inclined equiaxed dendrites growing under forced convection by phase-field-lattice Boltzmann method[J]. *Journal of Crystal Growth*, 2018, **483**: 147 - 155. DOI:10.1016/j.jcrysgro.2017.11.029.

基于 PF-LBM 背景速度场对单晶核凝固生长的影响

梁文清[1,2,3] 雷 刚[2] 苟其宁[4] 疏志勇[1,3] 王天祥[2]

钱 华[1] 赵东亮[1] 郑晓红[1]

([1]东南大学能源与环境学院, 南京 210096)

([2]航天低温推进剂技术国家重点实验室, 北京 100028)

([3]航天低温推进剂技术国家重点实验室东南大学基地, 南京 210096)

([4]山东非金属材料研究所, 济南 250031)

摘要:在自然环境和工业系统中为了促进/抑制冰的形成,采用相场-粒子玻尔兹曼方法模拟了冰单晶核的生长演化过程,并分析背景流场条件对单晶核晶枝生长的影响.结果表明:背景流场使枝晶生长呈现不对称形状,即迎流侧的单晶核晶枝远比背流侧晶枝发达;迎流侧晶枝顶端生长速率远大于背流侧的枝晶生长速率,上游侧的晶枝尖端半径大于背流侧的晶枝尖端半径;在有背景流场条件下,单晶核的固相比大于无背景流场.背景流场的流速越高,迎流侧枝晶越发达,枝晶生长速度越快,枝晶尖端生长速度也越快.背流侧的流场流速较低,过冷度低于迎流侧,抑制了凝固过程,生长速度较慢,枝晶生长受到抑制.

关键词:单晶核;耦合速度场;模拟;格子玻尔兹曼方法

中图分类号:TK91